Available online at www.sciencedirect.com
SCIENCE DIRECT®
Journal of Solid State Chemistry 178 (2005) 2959–2972
JOURNAL OF SOLID STATE CHEMISTRY
www.elsevier.com/locate/jssc

Inherent instabilities of some W_5Si_3-type binary phases with large electropositive metal atoms: Six examples in the Ba–Pb, Ca–Sn–Mg,Cu,Zn, and La–Ga–Al,Zn systems

Ashok K. Ganguli[a,b], Shalabh Gupta[a,b], Jing-Tae Zhao[a,c], E. Alejandro Leon-Escamilla[a], John D. Corbett[a,*]

[a]*Ames Laboratory[1] and Department of Chemistry, Iowa State University, Ames, IA 50011, USA*
[b]*Department of Chemistry, Indian Institute of Technology, New Delhi 110016, India*
[c]*Shanghai Institute of Ceramics, Shanghai 200050, China*

Received 14 May 2005; received in revised form 23 June 2005; accepted 28 June 2005
Available online 15 August 2005

Abstract

A particular pathology of certain W_5Si_3-type A_5B_3 structures ($I4/mcm$) appears to arise because of unduly close approaches of the $A1$-type atoms on the cell faces at $\frac{1}{2}$, 0, ($\frac{1}{4}$, $\frac{3}{4}$) that occur with the larger and more electropositive A and/or in the presence of smaller B atoms. A structure refinement of binary $Ba_{4.81}Pb_3$ indicates such a marginal stability in that the Ba atoms in the facial $Ba_{0.81}$ chains exhibit an extreme displacement ellipsoid along $\vec{c}$. Although Ca_5Sn_3 and La_5Ga_3 binaries are unknown in this structure type, five stable ternary derivatives of these have been synthesized via substitution reactions and characterized by single crystal X-ray diffraction means: $Ca_4Sn_{3.223(4)}Mg_{0.777}$, $Ca_4Sn_3Cu_{1.30(4)}$, $Ca_{4.66(6)}Sn_3Zn_{0.704(4)}$, $La_{4.81(1)}Ga_{1.38(2)}Al_{1.62}$, and $La_{4.762(5)}Ga_{1.5(1)}Zn_{1.5}$. Only the Ca–Sn–Zn phase exhibits lower symmetry, $P4/mbm$. The problematic $A1$ sites exhibit diverse changes in these, whereas the surrounding $B2$ tetrahedra are largely unaltered. The Ca–Sn results are, respectively: direct Mg/Sn substitution at the Ca1 site; mixed fractional distribution of the smaller Cu at two sites around the $A1$ position with an unresolved disorder; a pair of apparently independent modes, fractional Ca in the normal position and fractional Zn rectangles thereabout. The two La–Sn phases contain normal Ga,Al (Ga,Zn) tetrahedral chains with pairs of fractional disordered La atoms along $\frac{1}{2}$, 0, z. Each can be rationalized in terms of a reasonable incommensurate structure. Electronic effects may also be operable.

Keywords: W_5Si_3 structure; Crystal structure; Structural instability; Ba_5Pb_3 problems; Ca_5Sn_3 problems; La_5Ga_3 problems

1. Introduction

Interest in 5:3 compounds in binary intermetallic systems has existed for decades [1–3], and a great deal of research has been done recently on derivatives of such A_5B_3 phases. Among these are those with the hexagonal Mn_5Si_3 structure type that contain, in part, confacial chains of trigonal antiprisms of Mn with the basal edges edge-bridged by Si. Ternary examples of particular interest and relevance here are the many Mn_5Si_3Z types that are interstitial (stuffed) derivatives of the parent structure. Several hosts have been studied more thoroughly and found to be stable for a wide range of Z [4–7]. A second important group of 5:3 phases occurs in the tetragonal Cr_5B_3 structure (e.g., Ca_5Si_3, Ca_5Ge_3), and many of this type with tetrel components have been found to take up, or occur only with, hydride or fluoride

*Corresponding author. Fax: +515 294 6789.
E-mail address: jcorbett@iastate.edu (J.D. Corbett).
[1]This research was supported by the Office of the Basic Energy Sciences, Materials Sciences Division, US Department of Energy, DOE. The Ames Laboratory is operated for DOE by Iowa State University under Contract No. W-7405-Eng-82. Accordingly, the US Government retains a nonexclusive, royalty-free license to publish or reproduce the published form of the contribution, or to allow other to do so for US Government purpose.

0022-4596/$ - see front matter © 2005 Elsevier Inc. All rights reserved.
doi:10.1016/j.jssc.2005.06.044

interstitials [8,9]. Thirdly, a less common binary 5:3 structure type was originally identified as the orthorhombic β-Yb_5Sb_3 type but, similarly, all nine known examples between dipositive metals Ca, Sr, Eu, or Yb and Sb or Bi have been shown to also be hydrides with the Ca_5Sb_3F structure [10]. (The situation with trivalent cations in this structure type is not as clear.)

Finally, the well-studied body-centered-tetragonal W_5Si_3 structure [3] occurs for a substantial variety of compounds that involve mainly group 3–6 transition metals with main group 3–5 (13–15) metals and metalloids. Briefly, the basic structure (Fig. 1) consists of a body-centered array of columns of confacial square antiprisms of W2 (Wykoff 16*g*) along $\vec{c}$ in which each antiprismatic column is centered by a commensurate chain of generally smaller Si1 (4*a*) atoms. These columns are interconnected by parallel and commensurate chains of Si2 (8*h*) tetrahedra that share edges along $\vec{c}$, are centered in the W1 atoms (4*b*), and lie around the side (*a*–*c*, *b*–*c*) faces of the cell. These W1 sites exhibit relatively short separations for the more electropositive component, 2. 49 Å (*c*/2) in the parent [2,3] and ~2.54 Å in $(Nb,Ta)_5Si_3$ [11], and these positions are the focus of particular problems reported here when occupied by relatively larger group 2 or 3 atoms (Ba, Ca, La), especially when the post-transition element is relatively small (Ga).

Substituted ternary examples offer more variety and novel effects. First, substitution of about one-half of later mainly 3d metals *M* for Si1-type atoms that center the antiprismatic chains is found among isopointal $A_5B_{3-x}M_x$ parents with A = Ti, Zr, Hf, B = Sn, Sb, Bi

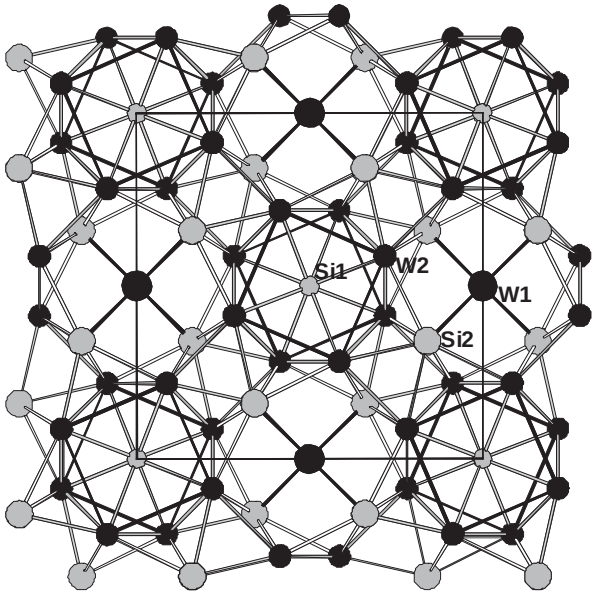

Fig. 1. [001] view of the W_5Si_3 structure. Sizes and colors: W1: large, black; W2: medium black; Si1: medium gray; Si2: large gray. Note chains of Si1-centered square antiprisms of W2 and chains of edge-sharing Si2 tetrahedra centered by W1 atoms on the cell faces.

[12–15] and others, evidently for bonding reasons. Generally, these do not concern us here except for two examples with analogously short Zr–Zr or Hf–Hf separations in the W1 positions, as follows. Although Zr_5Si_3 and Hf_5Si_3 do not appear to exist with W_5Si_3-like structures, electron-richer antimony derivatives with Fe substituting in the Si1 positions in the antiprism chain are found in ~$Zr_5Sb_{2.55}Fe_{0.45}$ [12] and ~$Hf_5Sb_{2.67}Fe_{0.33}$ [13]. The resultant (Zr,Hf)1–(Zr,Hf)1 distances, 2.75 Å, compare with 2.88–2.90 Å for standard single bond metal distances for these two [16] and 3.20–3.40 Å for *d*(Zr2–Zr2) in the trigonal antiprisms in the former.

We have found more pathological problems exist with certain prospective W_5Si_3-type compounds that consist of main group tetrels or triels combined with larger electropositive metals. The only hint of this problem in the literature occurs for Eu_5Sn_3 [17]. Here the Eu1 (4*b*) atoms centered at $z = \frac{1}{4}, \frac{3}{4}$ on the side faces of the cell (within Sn tetrahedra) refine with an extreme displacement ellipsoid along $\vec{c}$, namely a U_{33}/U_{11} ratio of 22 and with no resolvable peak positions therein. (An occupancy refinement was abandoned after this led to residual peaks within the ellipsoid figure.) Some type of incommensurate disorder associated with Eu1 vacancies would seem to be a reasonable explanation. We have been brought to the present article by three separate observations of similar or related pathologies in our laboratories that have extended over some time. All involve W_5Si_3-type structures with alkaline-earth or rare-earth metals.

First, after three reported examples of Ba_5Pb_3 with a Cr_5B_3 structure were all shown to similarly result from formation of the hydride Ba_5Pb_3H [8]; careful exclusion of that tightly bound impurity gave evidently the first example of Ba_5Pb_3 with a W_5Si_3-type structure according to very consistent powder pattern data [9]. However, attempts at its structural refinement revealed problems that were suggestive of a marginal phase stability, in this case a fractional occupancy and extremely elongated ellipsoids for Ba1. The second and most recent example pertains to the nonexistence of Ca_5Sn_3 with a W_5Si_3 or any other 5–3 structure type. Such a composition but with a Cr_5B_3-type structure was included in a recent phase diagram result, but the authors suspected this might be a hydride [18], and this stability condition was confirmed shortly thereafter [8]. Our conjecture following many unsuccessful attempts to prepare Ca_5Sn_3 was that repulsion between the equivalent Ca1 atoms was simply too severe, although the presence of the nearby $Ca_{31}Sn_{20}$ (= $Ca_{4.65}Sn_3$) composition with what has been described as a very distorted W_5Si_3-type structure [19] may contribute to the instability. (The same relationship applies in Sr–Pb.) In this case, substitutions of smaller elements for Ca1 were found to yield the desired structure type but with some complexities. An analogous example and some incommensurate superstruc-

tures have been analyzed for $Ae_{\sim 0.6}K_4Te_3$ (Ae = Ca, Sr) in this structure type [20].

Thirdly, our earlier explorations of the hexagonal Mn_5Si_3-type R_5Ga_3 phases showed that some of the earlier lanthanides R exhibit this structure type at least at higher temperatures, with a Ba_5Si_3-type (distorted Cr_5B_3) forming either at lower temperatures or for later R elements [21], but we saw none of the W_5Si_3-type phases occasionally reported in the literature. On the other hand, La_5Sn_3 derivatives with a larger and electron-richer B element are stable in this structure [22]. Subsequent explorations of a possible interstitial chemistry in the hexagonal R_5Ga_3 members turned up instead of a number of evident substitution products with tetrel, pnictogen and chalcogen elements on Ga sites [23]. On the other hand, the addition of modest amounts of earlier and smaller late transition or main group elements surprisingly produced W_5Si_3-type structures instead, as reported here. However, it should be noted that these examples also involve appreciably higher electron counts ($e/a \sim 3$) than the others ($e/a \sim 2$).

These three areas may all be imagined to have a common cause or explanation, that compounds containing a relatively larger and more polar group 2 or 3 metal in the $M1$ position on the side faces of the W_5Si_3-type structure are unstable or only marginally stable. This can be particularly exaggerated with a relatively small post-transition B element such as gallium. In these cases a W_5Si_3-type structure occurs only when up to 20% of the more active A component is replaced by a smaller metal, although at times this substitution may lead to fractional, alternate $M1$ site occupation, with or without appreciable disorder. Some of the results are suggestive of incommensurate structures or undetected superstructures, which will be the subjects of future research.

2. Experimental section

2.1. Syntheses

The compounds were synthesized from high-purity elements. Dendritic Ca and Ba (99.9%, 99.8%, APL Materials or Alfa-Aesar), Sn bar (99.99% Baker analyzed), Pb (99.999% Aesar), Ga (99.999%, Johnson–Matthey), Al wire (99.99%, United Mineral and Chem.), Zn granules (99.999%, J.T. Baker), Cu and Mg turnings (99.99%, Ames Laboratory) were used for the syntheses. In most cases, stoichiometric amounts of the elements were loaded in a Ta tube container inside a He-filled glovebox. The Ta tubes were welded on the second end, jacketed in evacuated and baked fused silica containers, and heated in resistance furnaces. The more routine synthesis data are detailed in Table 1. In other specifics, the Ba–Pb phase was prepared from reactions of the elements under dynamic vacuum at 1150 °C followed by slow cooling to 650 °C. The silica jacket was in this case connected to a high-vacuum system so as to remove impurity hydrogen. Materials prepared under these conditions consistently gave single-phase products (>95%) with Guinier patterns characteristic of the W_5Si_3-type structure. The tetragonal Ca–Sn–Cu phase is not of fixed composition. Different loading proportions, which may not cover the entire range, result in variation of lattice parameters from 12.588 to 12.758 Å in a and from 6.129 to 5.941 Å in c, respectively, as the Sn:Cu proportion increases. The Ca–Sn–Zn compound appeared to be a line phase. The lack of a high-yield synthesis of the Ca–Sn–Mg phase probably arises because of an undiscovered peritectic decomposition. The La–Ga–Z mixtures were typically prereacted around 400 °C to avoid Ga attack of the Ta container. More electronegative elements such as C, N, O gave neither substitution in a W_5Si_3-type structure nor an interstitial role in an Mn_5Si_3-type product. All of the products are black.

Table 1
Synthesis reaction conditions[a]

Phase	Method[b]	Equilibration (°C)	Product type (yield)[c]	e/a
$Ba_{4.81}Pb_3$[d]	D	1150°, 6–8 h; SC, 10°/h to 650°	>95% W	2.0
$Ca_4Sn_{3.22}Mg_{0.78}$	S	930°, 10 h, Q; 850°, 10 d	~50% W, 50% C	2.0
$Ca_4Sn_3Cu_{1.30}$	S	930°, 10 h; Q	>90% W	1.84
$Ca_{4.66}Sn_3Zn_{0.70}$[e]	S	930°, 10 h; Q	>95% W[e]	2.0
$La_{4.81}Ga_{1.38}Al_{1.62}$[f]	S	550°, 30 h	~80% W	3.0
$La_{4.76}Ga_{1.5}Zn_{1.5}$[f]	S	550°, 30 h	~80% W	2.81

[a]Loaded on stoichiometry unless otherwise noted.
[b]Reaction method: S: SiO_2-jacketed Ta; D: dynamic vacuum in Ta; SC: slow cooling; Q: quench in water.
[c]W: W_5Si_3 type; C: Co_2Si-type ($Ca_{2-x}Mg_xSn$, Ref. [24]).
[d]Ref. [8].
[e]Lower symmetry $P4/mbm$.
[f]Loaded as $La_{4.5}Ga_{1.5}Z_{1.5}$.

2.2. Powder X-ray diffraction

All reactants and products were handled in nitrogen-filled glove boxes. X-ray powder diffraction studies of the La–Ga–Z and Ba–Pb systems were carried out with the aid of an Enraf–Nonius Guinier camera, Cu$K\alpha_1$ radiation and NIST Si as an internal standard on samples contained between sheets of cellophane tape [10,24]. Unit cell parameters were calculated from least-squares refinement of indexed 2θ values. X-ray powder diffraction studies on Ca–Sn–Z systems were carried out on samples mounted between two layers of Mylar sheet with the help of a little vacuum grease. This sample holder was mounted on a Huber 670 Guinier powder camera equipped with a position-sensitive detector and

Cu$K\alpha_1$ radiation ($\lambda = 1.540598$ Å). The step size was set to 0.005°, and the exposure time was 45 min. High-quality cell parameters were obtained by a least-squares fit to the observed d values with the aid of the Rietica software [25].

2.3. Single crystal structure determinations

General data for the six refined structures are listed in Table 2. All single crystals were selected under low magnification and mounted in thin-walled glass capillaries in a glovebox designed for this purpose. Diffraction data for Ba–Pb and La–Ga–Z crystals were collected on CAD-4 or Rigaku AFC6R diffractometers. Absorption corrections were applied according to three psi-scans and, sometimes, subsequently at the isotropic stage with the aid of DIFABS [26]. Direct methods (SHELXS-86) [27] were used when necessary to develop models, and data were refined with the TEXSAN program package [28].

Table 2
Crystal and structure refinement data for W_5Si_3-type phases

Empirical formula	$Ca_4Sn_{3.223(4)}Zn_{0.777(4)}$	$Ca_4Sn_3Cu_{1.30(4)}$	$Ca_{4.66(6)}Sn_3Zn_{0.704(4)}$
Formula weight	564.29	595.82	595.48
Temperature (K)	293(2)	293(2)	293(2)
Crystal systems	Tetragonal	Tetragonal	Tetragonal
Space group, Z	$I4/mcm$ (No. 140), 4	$I4/mcm$, 4	$P4/mbm$ (No. 127), 4
Unit cell dimension (Å, Å^3)			
a	12.4062(7)	12.659(3)	12.5945(14)
c	6.0852(7)	6.050(3)	6.1329(13)
V	936.60(13)	969.5(5)	972.8(3)
c/a	0.4905	0.4779	0.4870
Density (calc.) (Mg/m^3)	4.002	4.082	4.066
Absorp. coeffic. (mm^{-1}) (Mo$K\alpha$)	10.737	12.363	11.864
Crystal size (mm^3)	$0.12 \times 0.09 \times 0.04$	$0.10 \times 0.08 \times 0.06$	$0.10 \times 0.08 \times 0.06$
Theta range for data collec. (deg)	2.32–28.26	2.28–28.15	2.29–28.28
Index ranges	$-16 \leqslant h \leqslant 15$, $-7 \geqslant k \geqslant 15$, $-7 \geqslant l \geqslant 7$	$-16 \leqslant h \leqslant 13$, $-16 \leqslant k \leqslant 16$, $-7 \leqslant l \leqslant 8$	$-16 \leqslant h \leqslant 16$, $-16 \leqslant k \leqslant 16$, $-7 \leqslant l \leqslant 8$
Reflections collected	2806	2684	8073
Indep. reflect. [R(int)]	332 [0.281]	346 [0.0332]	692 [0.0751]
Completeness (%)	96.8	98.9	97.9
Data/restraints/parameters	332/0/17	346/0/23	692/0/37
Goodness-of-fit on F^2	1.085	1.162	1.043
Final R indices [$I > 2\sigma(I)$]:			
R_1, wR_2	0.0165, 0.0361	0.0367, 0.0991	0.040, 0.0914
(all data)	0.0188, 0.0366	0.0400, 0.1002	0.0587, 0.0987
Extinction coefficient	0.0006(1)	0.000(4)	0.0000(3)
Largest diff. peak and hole (e/A^3)	0.596, −0.502	3.310, –1.146	2.038, –1.563
Empirical formula	$Ba_{4.82(2)}Pb_3$	$La_{4.81(1)}Ga_{1.38(2)}Al_{1.62(2)}$	$La_{4.762(5)}Ga_{1.5(1)}Zn_{1.5(1)}$
Formula weight	1282.1	807.63	869.40
Temperature (K)	294	294	223
Crystal system	Tetragonal	Tetragonal	Tetragonal
Space group, Z	$I4/mcm$ (No. 140), 4	$I4/mcm$ (No. 140), 4	$I4/mcm$ (No. 140), 4
Unit cell dimension (Å, Å^3)			
a	14.148(2)	12.790(5)	12.778(2)
c	6.4288(9)	5.546(3)	5.480(2)
V	1286.8(4)	907.2(8)	894.8(5)
c/a	0.4544	0.4336	0.4289
Density (calc.) (Mg/m^3)	6.752	5.912	6.453
Absorp. coeffic. (mm^{-1}) (Mo$K\alpha$)	54.413	26.318	30.893
Crystal size (mm^3)			
Theta range for data collec. (deg)		2–50	2–50
Index ranges	h, k, l	h, k, l	h, k, l
Reflections collected	2208	1773	1650
Indepen. reflect. [R(int)]	328 [0.20]	276 [0.082]	209 [0.108]
Data/restraints/parameters	328/0/18	276/0/22	209/0/21
Goodness-of-fit on F^2	2.14	2.06	2.19
Final R indices [$I > 3\sigma(I)$]:			
R, R_w	0.049, 0.055	0.034, 0.032	0.030, 0.039
Extinction coefficient	$1.1(2) \times 10^{-7}$	$5.2(4) \times 10^{-7}$	$9.7(3) \times 10^{-7}$
Largest diff. peak and hole (e/Å^3)	3.45, –2.98	2.66, –1.90	2.58, –186

The quality and singularity of the Ba_5Pb_3 crystals were tested through oscillation photographs. Reflection data were collected for almost one hemisphere and for a primitive tetragonal cell. The structure was solved in the highest symmetry group of the indicated body-centered group. Anisotropic refinement revealed one very troublesome Ba atom position, Ba1. An extreme displacement ellipsoid ratio along $\vec{c}$ of ca. 52 (U_{33}/U_{11}) was calculated prior to atom occupancy refinement. After full refinement, the ellipsoid displacements for this atom became more extreme, but the refinement statistics improved measurably. A formula of $Ba_{4.81(2)}Pb_{3.00(1)}$ was calculated for the compound. Attempts to solve the structure in the lower symmetry space groups *I*42*d* (No. 122), *I*4*cm* (No. 108) and *Iba*2 (No. 45) resulted in either smaller displacements with worse statistics or unstable solutions.

The CCD data for the Ca–Sn–*Z* samples were obtained from three sets of 606 frames obtained with 0.3° scans and exposure times of 10 s per frame over a 2θ range of ~3–57°. The intensities were integrated using the SAINT program in the SMART software package [29]. The data were corrected for Lorentz, polarization and for absorption effects empirically by the program SADABS [30]. The structures were solved by direct methods and refined by full matrix least-squares refinements on F_0^2 using the Bruker SHELXTL 6.1 software package [31].

The observed extinction and the intensity statistics for the Ca–Sn–Mg,Cu products were consistent with the *I*4/*mcm* space group. Direct methods provided four positions for the Mg phase and five for the Cu compound (two Sn, two Cu and one Ca). The solution and refinement of the Mg structure appeared routine, with the Ca1 position in the hypothetical binary being occupied by a mixture of Mg and Sn (~78:22) assuming full occupancy. However, an admixture of 22% Sn with Mg on the problem site may seem unusual. The binary composition $Ca_{4.946(5)}Sn_{3.0535}$ may be refined about as well ($wR_2 = 0.039$) but with about 5.3(5)% Sn on the nominal Ca1 (or Mg) site and a thermal ellipsoid about twice as large as for the other regular atom. Less than 30% Sn alone will also refine on this site and of course a corresponding 100% occupancy by fractions of Ca plus Sn can also be refined here. However, the pure binary has never been made, and Mg is always required for the formation of this structure, as verified by Energy dispersive spectroscopic (EDS) data (below). In the Cu phase, the isotropic displacement parameters were large for both types of Cu atoms, and they were also close neighbors, but refinement of their occupancies led to partial values for both. Both the copper sites were checked for (irregular) mixed occupancy by Ca atoms, but this did not give any significant improvements, the choice of Cu also being guided by the EDS data (below). The refinement converged to $R_1/wR_2 = 3.7/9.9\%$. The final refinement involving 346 unique reflections and 23 variables led to a composition of $Ca_4Sn_3Cu_{1.30(4)}$. The minor Cu site refined with a very elongated ellipsoid, but a Fourier map showed an atom-like peak at the refined position. Data were collected and refined for two different Cu crystals from the same reaction with similar results. The observed Guinier powder pattern agreed well with that calculated according to the refined structural parameters.

Data for the Ca–Sn–Zn product were first collected on a CAD-4 diffractometer. Systematic absences indicated space groups *P*4/*mbm*, *P*4*bm* or *P*$\bar{4}$*b*2. The centrosymmetric space group *P*4/*mbm* was selected initially, and the structure refined smoothly in this space group to $R/R_w = 3.4/3.3\%$. One of the Ca and one of the Zn sites were each found to be partially occupied and with short distances between them. The final refined composition was $Ca_{4.66(2)}$ $Sn_3Zn_{0.704(4)}$. Another X-ray dataset was later collected on the CCD instrument from a crystal obtained from a different reaction run under identical synthetic conditions, and its parallel refinement led to a composition of $Ca_{4.65(6)}Sn_3Zn_{0.70(4)}$, very similar to, but not as precise as, that obtained from CAD-4 data. The calculated and observed Guinier powder patterns agreed very well.

These results may be a manifestation of an incommensurate or superstructure, although a 7-day exposure (Cu$K\alpha$) with the crystal aligned along the *c*-axis in an oscillation camera did not reveal any superstructure spots. None was clearly observed in the CCD frames of the (0*kl*) and (*h*0*l*) zones secured with a 500 second exposure time for each either. Refinements were also attempted in the non-centrosymmetric space groups *P*$\bar{4}$*bm* and *P*4$\bar{b}$2. However, these did not affect the close and fractionally occupied positions.

2.4. EDS studies

The three Ca–Sn–*Z* crystals from which X-ray data had been collected were transferred to a JEOL 840A Scanning Electron Microscope equipped with IXRF Systems iridium X-ray analyzer. Care was taken to transfer the crystals via a Hexland transfer chamber filled with nitrogen. The average compositions (from four different spots on each single crystal) were $Ca_{3.44(7)}Sn_{3.2(4)}Mg_{0.34(4)}$, $Ca_{4.83(2)}Sn_{3.000(5)}Cu_{0.92(3)}$, and $Ca_{4.9(2)}Sn_{3.00(3)}Zn_{0.65(2)}$ when normalized to the refined Sn coefficients. These values are reasonable on comparison with the refined compositions $Ca_4Sn_{3.223(4)}Mg_{0.77(4)}$, $Ca_4Sn_3Cu_{1.30(4)}$, $Ca_{4.66(1)}Sn_3Zn_{0.70(1)}$ keeping in mind possible errors introduced by the irregular shape of the crystals and the presence of minor amount of grease on the samples. The EDS studies did confirm that a third element Zn, Cu or Mg is essential for the stabilization of the three W_5Si_3-type structures that contain Ca and Sn as the major components.

2.5. Physical property measurements

Electrical resistivities were measured by the electrodeless "Q" method with the aid of a Hewlett–Packard 4342A Q meter [32]. The method is particularly suitable for measurements on air sensitive samples. For this purpose, ~100 mg of $Ca_{4.78(2)}Sn_3Zn_{0.70(2)}$ was sealed in Pyrex tubes mixed with chromatographic-grade alumina. The sample was first carefully sieved such that the grains were in the range of 150–250 μm. Measurements were obtained at 34 MHz over the temperature range of 80–260 K. The results establish that the phase is metallic, as might be expected, with an extrapolated ρ_{293} of ~1120 μΩ cm. and a temperature dependence of 0.56% K^{-1}. Magnetic susceptibility data were obtained from the same reaction product that had been sealed under He in the container type described elsewhere [33]. The measurements were carried out over the range of 2–350 K on a Quantum Design MPMS SQUID magnetometer. The measured values were corrected for the container and for diamagnetism of the ion cores. The magnetic susceptibility results are shown in Fig. 2. A paramagnetic property is observed as the magnetization increases linearly as a function of the magnetic field, without evidence of paramagnetic impurities (Fig. 2a). The variation of the magnetic susceptibility with temperature is Pauli-like and nearly independent of the field (at the two fields studied) over a large range of temperatures (Fig. 2b).

3. Results and discussion

The W_5Si_3 structure consists of square antiprisms of W2 that share square faces to form an infinite chain, with Si1 atoms at the center of every square antiprism. These infinite chains are centered at the corners and center of the body-centered tetragonal unit cell and interconnected by Si2 atoms. More relevant to this study are chains of W1-centered tetrahedra built of Si2 along the sides of the unit cell and parallel to the *c*-axis (Fig. 1). The W1–W1-type distances are customarily short in many examples of this structure, often below "normal" "W–W" distances. This feature appears to become limiting or destabilizing with the larger active metals, as demonstrated here in some Ba, Ca and La systems.

3.1. Ba–Pb system

As an introduction, the binary Ba_5Pb_3 affords a normal structure except for an extreme version of elongated ellipsoids for the Pb1 atoms in the chain in the cell faces along $\vec{c}$ relative to that reported for Eu_5Sn_3 [17] (see Introduction). The best solution exhibits fractional occupancy of Ba1 and U_{33}:U_{11} ratios for Pb1 and Ba1 of 0.81(2):1 and ~124:1, respectively.

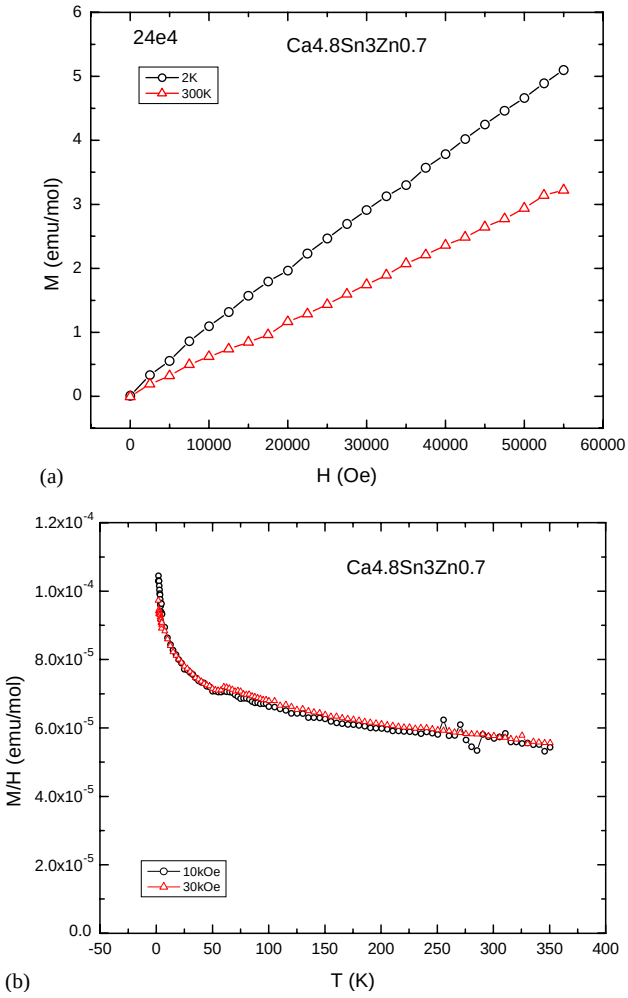

Fig. 2. Variations of (a) the magnetization (*M*) with applied magnetic field (*H*) and (b) the magnetic susceptibility with temperature for $Ca_{4.8}Sn_3Zn_{0.70}$.

Otherwise, the refinement is relatively respectable ($R, R_w = 4.9$, 5.5%, Table 2), and the two largest positive peaks in the final ΔF map, 3.45 and 3.23 $e^-/Å^3$, are 0.90 and 0.92 Å from Pb1 and Pb2, respectively, and the largest negative peak of 2.98 $e^-/Å^3$ is 0.7 Å from Ba1. Other structural data are given in Tables 3 and 4. Fig. 3 shows one cell face and the refined ellipsoidal features at the 70% probability level with the extreme asymmetry for Ba1. (The normal Ba2 atoms in front and back of the chain—compare Fig. 1—are omitted for clarity.) The nominal Ba1–Ba1 distance in the chain on the face would be very short 3.214(1) Å, but this is conceptually ameliorated by a reduced Ba1 occupancy of 81(2)%. The metallic single bond Ba–Ba length is given as 3.96 Å [16] and, suggestively, the corresponding incommensurate Ba1–Ba1 spacing with 80% occupancy would be a reasonable 4.03 Å (i.e., for four atoms averaged over five sites). A small elongation of the Pb2 ellipsoids along *c* is reasonable, presumably following the Ba1 disorder. Two similar phases with W_5Si_3

structures are known only from Guinier powder data, Eu_5Pb_3 [8] and Sm_5Tl_3 [34,35], and these might be expected to refine similarly.

The structural result is the ideal W_5Si_3-type save for the defect Ba1 site and its extreme displacement parameter when the Ba1 distribution is fit to such a model. The Ba1–Pb2 bonds in the somewhat flattened tetrahedra are all the same, 3.58 Å, which interestingly compares with the metallic single bond sum of 3.48 Å (for an extreme heteratomic bond). The shortest Ba2–Ba2 contact in the slightly twisted antiprisms is a very plausible 3.91 Å. Naturally, the sizes of the constituent atoms Ba and Pb make this the largest of the W_5Si_3-type phases considered here, 32% more than $La_{4.66}Sn_3Zn_{0.7}$.

Table 3

(a) Positional parameters ($\times 10^4$) and U_{eq} ($Å^2 \times 10^2$) for $Ba_{4.81(1)}Pb_3$

Atom	Wyckoff	x	y	z	U_{eq}	Occup.
Pb1	4*a*	0	0	$\frac{1}{4}$	0.8(1)	1
Pb2	8*h*	3399(1)	$x+\frac{1}{2}$	0	2.1(1)	1
Ba1	4*b*	0	$\frac{1}{2}$	$\frac{1}{4}$	35(4)	0.81(2)
Ba2	16*k*	2183(2)	861(2)	0	1.0(1)	1

(b) Anistropic displacement parameters ($Å^2 \times 10^3$) for $Ba_{4.81(1)}Pb_3$

	U_{12}	U_{22}	U_{33}	U_{12}	U_{13}	U_{23}
Pb1	7(1)	7	11(1)	0	0	0
Pb2	11.5(9)	11.5	3.9(2)	7.6(9)	0	0
Ba1	8(2)	8	1030(103)	0	0	0
Ba2	6(1)	10(1)	18(1)	–3(1)	0	0

Table 4
Neighboring distances <4.5 Å in $Ba_{4.8}Pb_3$

Pb1–Pb1 × 2	3.2144(4)	Ba2–Ba2	3.914(4)
Pb1–Ba2 × 8	3.689(2)	Ba2–Ba2 × 2	4.033(3)
Pb2–Ba2	3.368(3)	Ba2–Ba2 × 2	4.163(3)
Pb2–Ba2 × 4	3.793(1)	Ba2–Ba1 × 2	4.467(2)
Pb2–Ba2 × 2	3.885(2)	Ba1–Ba1 × 2	3.2144(4)
Pb2–Ba1 × 2	3.584(2)		

3.2. Ca_5Sn_3 system

Among the alkaline-earth tetrelides Ca_5Si_3 and Ca_5Ge_3 both crystallize with a Cr_5B_3-type structure [9,36], whereas the binary in the Ca–Pb system is apparently complex [33] and Ca_5Sn_3 does not exist. Our attempts to synthesize Ca_5Sn_3-type compounds always led to mixtures of Ca_2Sn, $Ca_{31}Sn_{20}$ and CaSn depending on the starting compositions and the reaction conditions. $Ca_{31}Sn_{20}$ has a stoichiometry very close to that of the missing Ca_5Sn_3.

Again, one reason for the apparent inability to synthesize certain W_5Si_3-type phases such as Ca_5Sn_3 could be the extremely short Ca1–Ca1 distances that this model would entail along the tetrahedral chain since this is constrained to ~3.0 Å ($c/2$), the same as the Sn–Sn distances along the center of the square antiprismatic columns. (The single bond distance for Ca is given as 3.47 Å [16] although it may be important that the present phase contains what could be considered as the partially oxidized metal.) In order to stabilize the desired 5:3 phase, we attempted to substitute smaller atoms (*M*) like Mg, Zn and Cu on the Ca1 site so that the (*M*–*M*) distances might become more reasonable and make the structure stable. All three work, with Mg providing the probably most straightforward result.

3.2.1. Ca–Sn–Mg system

With Mg, the tetrahedral chain apparently becomes centered by a mixture of Mg and Sn3 (~78:22 assuming full occupancy) instead of Ca1, a feature that affords uncrowded distances of 3.042 Å between these atoms along the tetrahedral chains (Tables 5 and 6, Fig. 4). Mg–Sn mixing has been noted in Ca–Rh–Sn systems as well [37]. The absence of fractional occupancies and disorder is reflected in the much lower *R* factors ($R_1/wR_2 = 0.0165/0.036$) here compared with the two that follow.

As simple as they may be, Pauling's single bond metallic radii [16] allow a rough and easy judgment as to what components may be tightly bonded in this

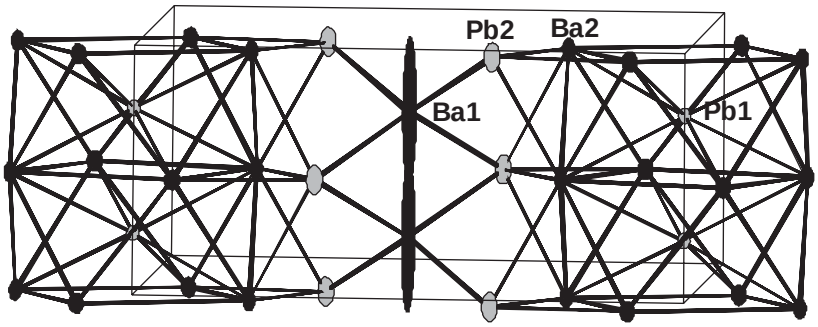

Fig. 3. [100] view of Ba2 square antiprisms centered by Pb1 and the disordered 0.81 Ba1 at $0,\frac{1}{2},\frac{1}{4}$, centered within Pb2 tetrahedra in $Ba_{4.81}Pb_3$. Anisotropic displacement ellipsoids are drawn at the 70% probability level. The atom shading scheme is the same as in Fig. 1.

Table 5

(a) Atomic coordinates ($\times 10^4$) and equivalent isotropic displacement parameters ($Å^2 \times 10^3$) for $Ca_4Sn_{3.223(4)}Mg_{0.777}$[a]

Atom	Wyckoff	x	y	z	U_{eq}	Occup.
Sn3	4*b*	0	$\frac{1}{2}$	$\frac{1}{4}$	21(1)	0.223(4)
Mg	4*b*	0	$\frac{1}{2}$	$\frac{1}{4}$	21(1)	0.777
Sn1	4*a*	0	0	$\frac{1}{4}$	13(1)	1
Sn2	8*h*	1536(1)	$\frac{1}{2}+x$	0	18(1)	1
Ca	16*k*	825(1)	2159(1)	0	17(1)	1

(b) Anisotropic displacement parameters ($Å^2 \times 10^3$) for $Ca_4Sn_{3.223(4)}Mg_{0.777}$[b]

Atom	U_{11}	U_{22}	U_{33}	U_{12}	U_{13}	U_{23}
Sn3	22(1)	22(1)	20(1)	0	0	0
Mg	22(1)	22(1)	20(1)	0	0	0
Sn1	13(1)	13(1)	14(1)	0	0	0
Sn2	14(1)	14(1)	27(1)	−1(1)	0	0
Ca	16(1)	14(1)	20(2)	−2(1)	0	0

[a] U_{eq} is defined as one third of the trace of the orthogonalized U_{jj} tensor.

[b] The anisotropic displacement factor exponent takes the form: $-2\pi^2[h^2a^{*2}U_{11} + \cdots + 2hka^*b^*U_{12}]$.

Table 6
Important bond lengths [Å] in $Ca_4Sn_{3.223(4)}Mg_{0.777}$

Mg,Sn3–Mg,Sn3	3.0426(4)
Sn2–Mg,Sn3	3.0946(4)
Sn2–Ca	3.347(1)
Sn2–Ca	3.364(1)
Sn1–Sn1	3.0426(4)
Ca–Sn1	3.2463(7)
Ca–Sn2	3.3467(9)
Ca1–Sn2	3.5573(5)
Ca–Ca	3.537(1)
Ca–Ca	3.667(1)
Ca–Ca	3.839(1)
Ca–Mg,Sn3	3.9726(8)

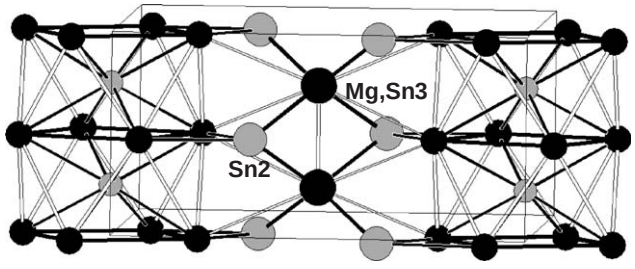

Fig. 4. Section about the [100] face of the structure of $Ca_4Sn_{3.223(4)}Mg_{0.777}$ showing the Sn2 tetrahedra (large gray) centered by disordered Mg,Sn3 atoms (black) (78:22) and the Sn1-centered square antiprismatic columns of Ca at the cell corners (smaller gray and black spheres).

structure. (However, we have demonstrated in other systems that distances may not always reflect just overlap population variations [38].) The shorter Ca–Ca contacts that remain, 3.54 and 3.67 Å, and the centering Ca–Sn1 distance 3.25 Å are reasonable with regard to the sums of the standard values, 3.47 and 3.16 Å, respectively, especially considering differences in the coordination environments. The Ca–Mg,Sn3 separations between the columns are in contrast relatively large. The Sn2 tetrahedron that surrounds the Mg,Sn3 sites has a radius of 3.095 Å, compared with the separate radius sums of 2.78 and 2.84 Å, respectively. The Mg,Sn3–Mg,Sn3 separations along $\vec{c}$ of 3.04 Å are large compared with the weighted metallic distance, 2.75 Å, as expected.

3.2.2. Ca–Sn–Cu system

A comparable W_5Si_3-type phase as described for Mg is also obtained in the Ca–Sn–Cu system (Table 7) in that there are no short bonds at the corresponding Ca1–Ca1 site. These $0, \frac{1}{2}, \frac{1}{4}$ positions are occupied by Cu1 atoms with relatively large separations of 3.025 and 3.217 Å for bonding to four Sn2 at 3.217 Å (2.35 Å is the radius sum). The Cu1 position is additionally 47(1)% occupied. However, a second apparent 16*j* Cu2 site (at x, 0, $\frac{1}{4}$) with only a 21(1)% occupancy is coplanar with Cu1 and generates a square around it. The composite, Fig. 5, requires some further thought. The short distances of 1.42 Å for Cu1–Cu2 and 2.01 Å for Cu2–Cu2, as the edges of the square are difficult to interpret (the radius sum is 2.35 Å), but a strong correlation between occupancies of the two Cu could avoid all unreasonable separations. No regular order in a supercell could be found with the CCD instrument, but an irregular disorder, an incommensurate structure,

Table 7

(a) Atomic coordinates ($\times 10^4$) and equivalent isotropic displacement parameters ($Å^2 \times 10^3$) for $Ca_4Sn_3Cu_{1.30(4)}$[a]

Atom	Wyckoff	x	y	z	U_{eq}	Occup.
Ca	16*h*	2138(1)	836(1)	0	22(1)	1
Sn1	4*a*	0	0	$\frac{1}{4}$	20(1)	1
Sn2	8*h*	3413(1)	$\frac{1}{2}+x$	0	24(1)	1
Cu1	4*b*	0	$\frac{1}{2}$	$\frac{1}{4}$	33(2)	0.47(1)
Cu2	16*j*	3877(7)	0	$\frac{1}{4}$	74(4)	0.208(6)

(b). Anisotropic displacement parameters ($Å^2 \times 10^3$) for $Ca_4Sn_3Cu_{1.30(4)}$[b]

	U_{11}	U_{22}	U_{33}	U_{12}	U_{13}	U_{23}
Ca	21(1)	20(1)	24(1)	−5(1)	0	0
Sn1	15(1)	15(1)	29(1)	0	0	0
Sn2	23(1)	23(1)	28(1)	−5(1)	0	0
Cu1	13(2)	13(2)	72(5)	0	0	0
Cu2	144(11)	47(5)	30(4)	0	27(5)	0

[a] U_{eq} is defined as one third of the trace of the orthogonalized U_{ij} tensor.

[b] The anisotropic displacement factor exponent takes the form: $-2\pi^2[h^2a^{*2}U_{11} + \cdots + 2hka^*b^*U_{12}]$.

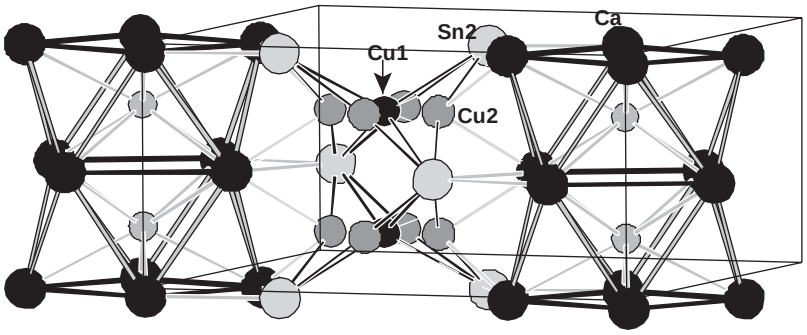

Fig. 5. [100] face section of the $Ca_4Sn_3Cu_{1.30}$ structure showing the disordered mixture of fractional Cu1 (black) and Cu2 (smaller gray) atoms around the cell face with normal Sn2 (large gray) forming tetrahedra.

Table 8
Bond lengths (Å) in $Ca_4Sn_3Cu_{1.30(4)}$[a]

Sn1–Sn1	3.025(1)
Sn1–Ca	3.277(2)
Sn2–Cu1	3.219(2)
Sn2–Cu2	2.582(2)
Sn2–Ca	3.336(2)
Sn2–Ca	3.465(2)
Ca–Cu2	2.872(7)
Ca–Ca	3.625(4)
Ca–Ca	3.692(2)
Ca–Ca	3.820(2)
Ca1–Cu1	3.025(1)
Cu1–Cu2	1.422(9)
Cu1–Cu2	3.34(1)
Cu2–Cu2	2.01(1)
Cu2–Cu2	2.84(2)

[a]Cu1 and Cu2 have fractional occupancies of 41 and 21%, respectively.

or intergrown microdomains are plausible. The higher proportion of copper in this compound may reflect its small size relative to either Mg (which is 0.20 Å larger in metallic radius) or Ca (0.52 Å), and its lower valence electron count ($e/a = 1.84$) may also be a factor. In fact, distances suggest that Cu2, with four times greater multiplicity and 64% of the total Cu, is the better bonded. Average Cu2 distances to neighboring atoms and the corresponding sums of metallic radii are very reasonable: to Ca, 2.87 Å (2.91 Å), and to Sn2, 2.58 Å (2.60 Å). We recognize that distances between atoms with low populations may not be very accurate, and Cu2's isotropic displacement parameter is large, 74×10^{-2} Å^2. On the other hand, Cu1 is quite distant from Ca, 4.06 Å, from Sn2, 3.22 Å, and even from itself, 3.025 Å. The disorder represented by the refined Cu1 position appears to reflect mainly an oversized cavity in the tetragonal Ca–Sn framework. We presume the refined result reflects some complex disorder, one that is not as easily imagined as for the three following structures (Table 8).

Table 9

(a) Atomic coordinates ($\times 10^4$) and equivalent isotropic displacement parameters (Å$^2 \times 10^3$) for $Ca_{4.66(1)}Sn_3Zn_{0.70(1)}$ (P4/mbm)[a]

Atom	Wyckoff	x	y	z	U_{eq}	Occup.
Ca1	8*i*	2181(2)	739(2)	0	21(1)	1
Ca2	8*i*	925(2)	2064(2)	$\frac{1}{2}$	24(1)	1
Ca3	4*f*	0	$\frac{1}{2}$	2303(10)	36(2)	0.655(7)
Sn1	4*e*	0	0	2481(2)	15(1)	1
Sn2	4*g*	3306(1)	$\frac{1}{2}+x$	0	27(1)	1
Sn3	4*h*	1456(1)	$\frac{1}{2}+x$	$\frac{1}{2}$	42(1)	1
Zn	8*k*	4301(2)	$\frac{1}{2}+x$	2844(7)	42(2)	0.349(6)

(b) Anisotropic displacement parameters (Å$^2 \times 10^3$) for $Ca_{4.66(1)}Sn_3Zn_{0.70(1)}$[b]

	U_{11}	U_{22}	U_{33}	U_{12}	U_{13}	U_{23}
Ca1	18(1)	24(1)	21(1)	−3(1)	0	0
Ca2	23(1)	29(1)	21(1)	10(1)	0	0
Ca3	18(2)	18(2)	72(5)	−1(2)	0	0
Sn1	15(1)	15(1)	13(1)	0	0	0
Sn2	26(1)	26(1)	30(1)	11(1)	0	0
Sn3	34(1)	34(1)	59(1)	−16(1)	0	0
Zn	49(2)	49(2)	28(2)	−25(2)	1(1)	1(1)

[a]U_{eq} is defined as one third of the trace of the orthogonalized U_{ij} tensor.

[b]The anisotropic displacement factor exponent takes the form: $-2\pi^2[h^2a^{*2}U_{11} + \cdots + 2hka^*b^*U_{12}]$.

3.2.3. Ca–Sn–Zn system

The more complex structure of $Ca_{4.66(1)}Sn_3Zn_{0.70(2)}$, Tables 9 and 10, is closely related to that of W_5Si_3 but has a lower symmetry, *P*4/*mbm* rather than *I*4/*mcm*. The body centering is lost, and the square antiprisms now defined by separate Ca1 and Ca2 atoms are slightly distorted and somewhat larger than before. The Sn1 sites near the centers of these are fully occupied and produce a linear chain parallel to the *c*-axis with alternating Sn1–Sn1 distances of 3.040 and 3.092 Å (Table 10, Fig. 6a). The Ca3 sites (in the former role of Ca1) near the center of the chains of tetrahedra defined by Sn2, Sn3 are partially occupied (66(1)%) in this

Table 10
Important bond lengths (Å) for $Ca_{4.66(1)}Sn_3Zn_{0.70(1)}$

Sn1–Sn1	3.043(2)	Ca2–Zn	3.125(4)
Sn1–Sn1	3.090(2)	Ca2–Sn1	3.240(2)
Sn1–Ca2	3.240(2)	Ca2–Sn3	3.387(3)
Sn1–Ca1	3.275(2)	Ca2–Sn3	3.530(2)
Sn2–Zn	2.487(4)	Ca2–Ca2	3.583(4)
Sn2–Ca1	3.290(2)	Ca2–Ca1	3.717(2)
Sn2–Ca3	3.332(3)	Ca3–Ca3	2.82(1)
Sn2–Ca1	3.376(2)	Ca3–Sn3	3.076(4)
Sn2–Ca2	3.576(1)	Ca3–Zn	3.393(7)
Sn3–Ca3	3.076(4)	Ca3–Zn	3.226(7)
Sn3–Zn	3.166(3)	Ca3–Zn	1.288(4)
Sn3–Ca2	3.386(3)	Ca3–Ca3	3.31(1)
Sn3–Ca3	3.076(2)	Ca3–Sn2	3.332(3)
Sn3–Ca1	3.628(1)	Ca3–Zn	3.393(7)
Ca1–Sn1	3.275(2)	Zn–Ca3	1.288(4)
Ca1–Sn2	3.290(2)	Zn–Zn	2.490(8)
Ca1–Sn3	3.628(1)	Zn–Zn	2.644(9)
Ca1–Zn	3.668(3)	Zn–Ca2	3.125(4)
Ca1–Ca1	3.705(4)	Zn–Ca3	3.226(7)
Ca1–Ca2	3.717(2)	Zn–Ca3	3.393(7)
Ca1–Ca2	3.833(2)	Zn–Sn2	2.487(4)
		Zn–Sn3	3.166(3)

[a]Ca3 and Zn have fractional occupancies of 66% and 35%, respectively.

model. The Ca3–Ca3 distances alternate at 2.82 and 3.31 Å, and correlations of the 66% occupancies, a disordered, or an incommensurate structure would leave no problem internally as far as the single bond distance used as a rough guide, ~3.47 Å. But we also find a pair of 35(1)%-occupied Zn sites close to Ca3 (at 1.29 Å), but slightly out of the plane, and these are drawn separately in Fig. 6b. The Zn appears to be strongly bound to Sn2 on the basis of distance (2.49 vs. 2.63 Å). The pairs of Sn3 atoms appear coplanar with but somewhat more weakly bound to Ca2 in the antiprismatic chains, but strongly bonded to Ca3, and this is presumably the source of the larger displacement parameter for Sn3. The fractional Ca3 and Zn atoms occupancies also sum to 101(1)% and their very short separation, 1.29 Å, indicates considerable occupancy correlation must be present between them as well. Each can be viewed as playing a role in a strongly bound fragment.

The tetrahedral chain may thus be usefully thought of as built of two defect fragments, one of Ca3-centered Sn2,3 tetrahedra, the Ca3–Sn3 distances also being short and the other component made of Zn–Sn2 (and Zn–Zn) bonding (Fig. 6a and b, respectively). The Zn and Sn2 atoms are included as small circles in Fig. 6a for visual reference, but the Ca3–Zn distances are 0.28 Å over the standard radius sum, and Ca3–Sn2, 0.16 Å longer. The reverse is true in Fig. 6b in which the Sn3 atoms are marked only for reference. It is important to note that the Sn2–Sn2 and Sn3–Sn3 axes are nearly perpendicular when viewed along $\vec{c}$, Fig. 6c, better describing how the two partial structures can be viewed separately with

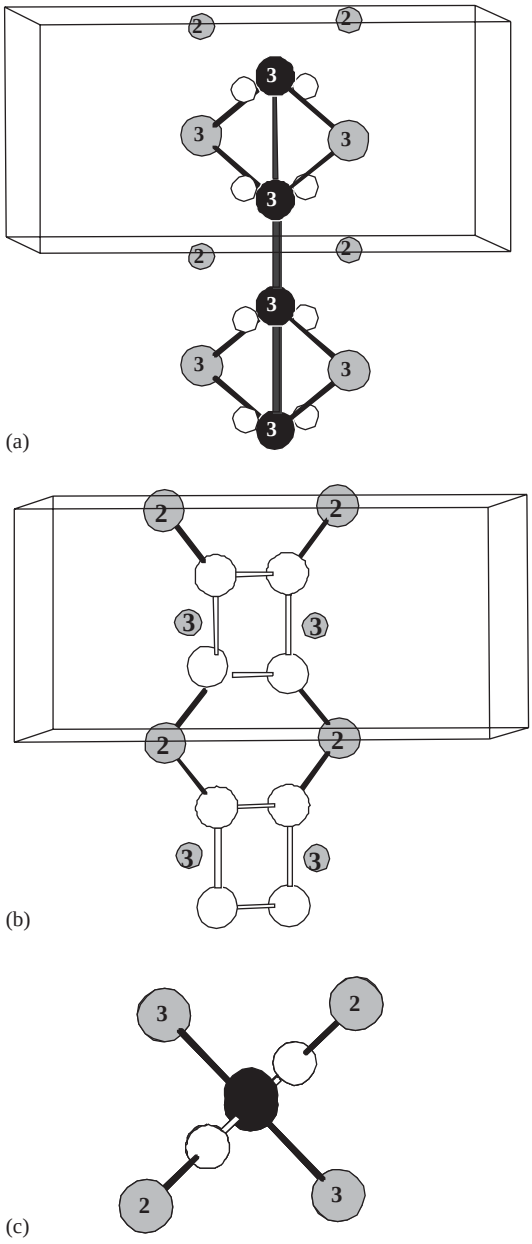

Fig. 6. Illustrations of the separate postulated tetrahedral chains along $\vec{c}$ in $Ca_{4.66}Sn_3Zn_{0.70}$ in terms of Sn (gray) and two partially occupied components (a) Ca3 (black) units and (b), Zn (white), each as judged by bond lengths. These chains are about normal to each other, as shown in a [001] view in (c). The smaller Zn and Sn circles are only to mark those atom positions in the other chain for reference. The normal square antiprismatic Ca, Sn1 chains at the edges are not shown.

some realism. The result seems preferable to an ideal centered tetragonal cell with full Ca occupancy of the side faces and tight separations of ~3.06 Å. The formation of an incommensurate structure (or intergrown slabs) seems a reasonable way to minimize the energy of the otherwise stressed system. An incommensurate superstructure model of a W_5Si_3 structure has been discussed earlier for the $Ae_xK_4Te_3$ (Ae = Ca, Sr) system [20].

3.3. La–Ga–Z systems, Z = Al, Zn

Although a phase $La_{\sim 5}Ga_{\sim 3}$ does not appear to exist in any structure, a double alteration again stabilizes W_5Si_3-type structures, namely a nearly 25% decrease in the La content and substitution of the nominally larger Al or Zn for at least half of the Ga that define the tetrahedra. As before, our targeted reduction of La1–La1 repulsions along $\vec{c}$ in the cell faces is accomplished. The normal La1 sites in both cases are split into two fractional sites that are quite disordered on the basis of the elemental cell and slightly different in the two cases, Figs. 7 and 8. No obvious superstructure was observed for either along $\vec{c}$ in the CAD-4 diffractometer data, although very weak satellite reflections might have been easily missed.

3.3.1. The La–Ga–Al system

In the Al derivative, ~45% substitution in the *X*2 sites (and ~72% in the antiprism *X*1 centers) leaves Ga as the minority component overall in $La_{4.81}Ga_{1.38}Al_{1.62}$. ($La_5Al_3$ is also unknown.) The antiprismatic chains are

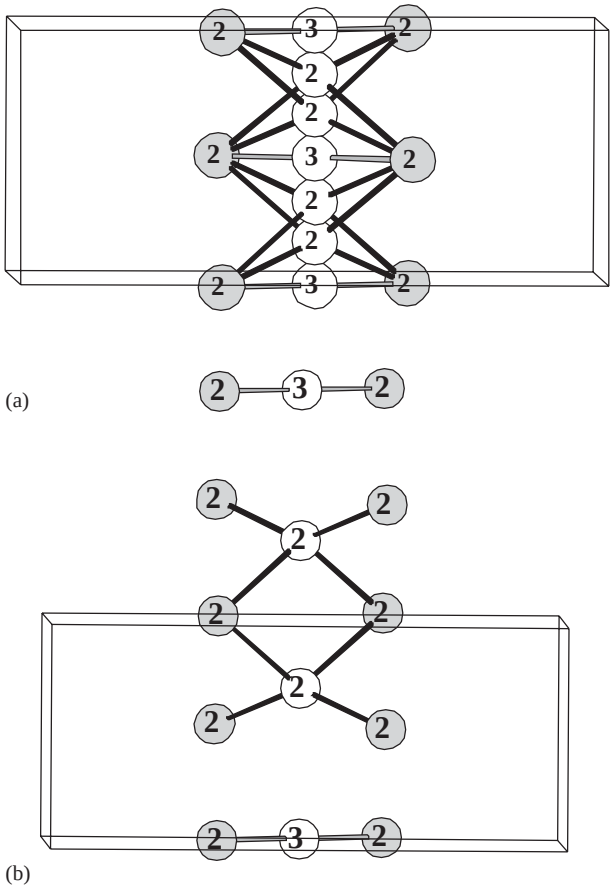

Fig. 7. (a) The tetrahedral chains in $La_{4.81}Ga_{1.38}Al_{1.62}$ showing the refined fractional La2,3 sites within the normal Ga2,Al2, tetrahedral sites. (b) One of four disordered La2,3 models proposed for the chain in a 2*c* cell.

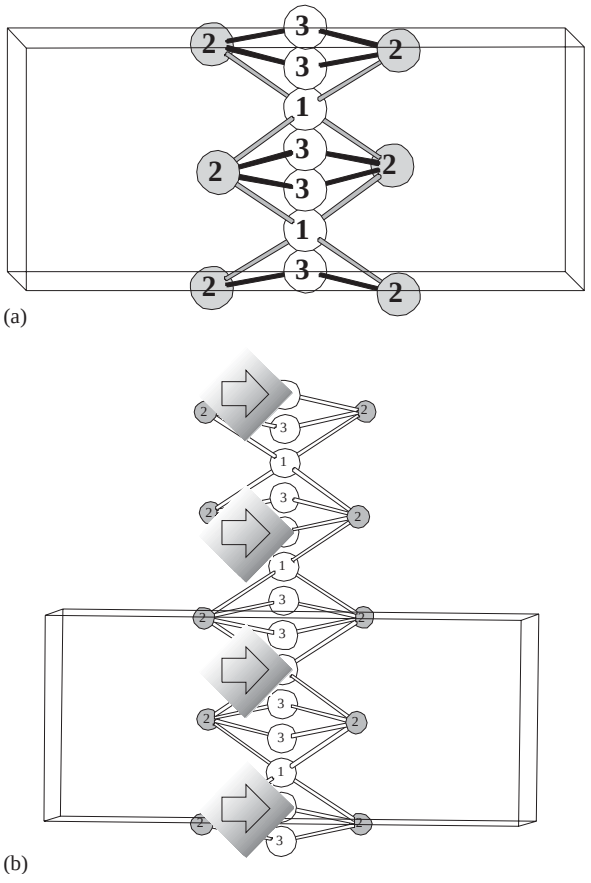

Fig. 8. (a) The refined fractional La1,3 positions within normal Ga2,Zn tetrahedra in $La_{4.76}Ga_{1.5}Zn_{1.5}$. (b) The proposed La1,3 disorder in a similar 2*c* cell is marked.

fairly normal. The typical chain of edge-sharing *X*2 tetrahedra are still present, but ~27% La occupies each of the independent 8*g* (La2) and 4*d* (La3) sites along 0, $\frac{1}{2}$, *z*, namely at $z = 0.171$ (0.329, 0.671, 0.829), and $\frac{1}{4}, \frac{3}{4}$, respectively (Table 11). Clearly, a considerable disorder or better, a superstructure or an incommensurate distribution of La1, is all that can be deduced from this X-ray refinement, Fig. 7a. (All La2 atoms that define the adjoining square antiprisms around the chains are omitted for clarity—compare Fig. 1.) This result is otherwise quite respectable (3.4, 3.2%) although the U_{33}/U_{11} ratios for the La2, 3 sites are 4.8 and 2.9, respectively, meaning the isotropic representation in the figure overstates the order refined. The split La2 (8*g*) positions still occur in distorted *X*2 tetrahedra (d(La2–*X*2) = 3.08 and 3.45 Å), whereas the minor La3 site is coplanar with two *X*2 atoms ($d = 2.93$ Å).

However, a reasonable superstructure model can be found when it is noted that all atoms in the 0, $\frac{1}{2}$, *z* string have ~25% occupancies. One possible set in a 2*c* cell is shown in Fig. 7b, in which every fourth atom has been selected. The La–La distances are now reasonable, 3.65 and 3.72 Å, for the refined atom centers as well as the La–*X*2 values. Three more displaced sets of the same

Table 11

(a) Positional parameters (× 10⁴) and U_{eq} (× 102) for $La_{4.81(1)}Ga_{1.38(2)}Al_{1.62}$

Atom	Wyckoff	x	y	z	U_{eq}	Occup.
La1	16*k*	2224.2(4)	854.8(5)	0	1.55(3)	1
La2	8*g*	0	$\frac{1}{2}$	1710(10)	2.9(3)	0.270(2)
La3	4*d*	0	$\frac{1}{2}$	0	4.4(2)	0.268(4)
Ga1,Al1	4*a*	0	0	$\frac{1}{4}$	1.7(1)	0.28(1)/0.72(1)
Ga2,Al2	8*h*	1621(1)	$\frac{1}{2}+x$	0	2.11(6)	0.55(1)/0.45(1)

(b) U values for $La_{4.81(1)}Ga_{1.38(2)}Al_{1.62}$

Atom	U_{11}	U_{22}	U_{33}	U_{12}	U_{13}	U_{23}
La1	1.34(3)	1.61(3)	1.67(4)	–0.14(2)	0	0
La2	1.3(2)	1.3(2)	6.2(4)	0	0	0
La3	2.7(2)	2.7	7.9(7)	–0.5(2)	0	0
Ga1, Al1	1.7(1)					
Ga2, Al2	2.11(6)					

Table 12
Interatomic distances (<4.5 Å) in $La_{4.81(1)}Ga_{1.38(2)}Al_{1.62}$[a]

La1–*X*2 × 2	3.291(1)	La2–La1 × 4	3.833(2)
La1–*X*2	3.319(2)	La2–La1 × 4	4.140(3)
La1–*X*1 × 2	3.348(1)	La3–La2 × 2	0.946(6)
La1–La1	3.475(2)	La3–La2 × 2	1.827(6)
La1–*X*2	3.494(2)	La3–La3 × 2	2.773(2)
La1–La1 × 2	3.531(2)	La3–*X*2 × 2	2.933(3)
La1–La3	3.715(2)	La3–La1 × 4	3.715(6)
La1–La1 × 2	3.718(2)	La3–La2 × 2	3.719(6)
La1–La2 × 2	3.833(2)	La3–*X*2 × 4	4.036(2)
La1–La1 × 2	4.140(3)		
La1–La1 × 2	4.310(2)	*X*1–*X*1 × 2	2.773(2)
La2 –La2	0.88(1)	*X*1–La1 × 8	3.348(1)
La2–La3	0.946(6)	*X*2–La3	2.933(3)
La2–La3	1.827(6)	*X*2–La2 × 2	3.081(3)
La2–La2	1.89(1)	*X*2–La1 × 4	3.291(1)
La2–La2 × 2	2.773(2)	*X*2–La2 × 2	3.319(2)
La2–*X*2 × 2	3.081(3)	*X*2–La2 × 2	3.455(4)
La2–*X*2 × 2	3.455(4)	*X*2–La1 × 2	3.494(2)
La2–La2	3.65(1)	*X*2–La3 × 2	4.036(2)
La2–La3	3.719(6)	*X*2–*X*2 × 2	4.218(1)

[a] *X* = mixed Ga–Al. La2 and La3 have fractional occupancies of ~27% each.

Table 13

(a) Positional parameters (× 10⁴) and U_{eq} (× 10²) for $La_{4.762(5)}Ga_{1.5(1)}Zn_{1.5}$

Atom	Wyckoff	x	y	z	U_{eq}	Occup.
La1	4*b*	0	$\frac{1}{2}$	$\frac{1}{4}$	1.9(3)	0.280(3)
La2	16*k*	2225.5(5)	873.5(5)	0	1.63(5)	1
La3	8*g*	0	$\frac{1}{2}$	830(10)	1.4(4)	0.241(2)
Ga1	4*a*	0	0	$\frac{1}{4}$	1.9(1)	1
Ga2	8*h*	3384(1)	$\frac{1}{2}+x$	0	1.3(2)	0.24(1)
Zn2	8*h*	3384	$\frac{1}{2}+x$	0	2.25(8)	0.76(1)

(b) U values (× 10²) for $La_{4.762(5)}Ga_{1.5(1)}Zn_{1.5}$

Atom	U_{11}	U_{22}	U_{33}	U_{12}	U_{13}	U_{23}
La1	1.5(2)	1.5	2.8(7)	0	0	0
La2	4.8(4)	1.75(4)	1.69(7)	–0.07(2)	0	0
La3	1.7(2)	1.7	0.7(7)	0	0	0
Ga1	1.63(7)	1.63	2.5(3)	0	0	0
Ga2	1.3(2)					
Zn2	2.26(8)					

sequence generate the observed result. The coplanar La3 site bears some resemblance to the defect site deduced for Ca in incommensurate isotypic $Ca_{0.6}K_4Te_3$ [20], namely on the shared edge between two tetrahedra (Table 12).

3.3.2. The La–Ga–Zn system

A similar loading for La–Ga–Zn gives a closely related result (Tables 13 and 14). In this case there is some understandable difficulty in differentiating Ga and Zn, but the best attempts gave the result $La_{4.76}Ga_{1.5}Zn_{1.5}$, consistent with the loaded composition $La_{4.8}Ga_{1.5}Zn_{1.5}$ and the high yield. The square antiprismatic columns centered by just Ga1 are normal as is the tetrahedral chain defined by the $Ga_{0.24}Zn_{0.76}$ (*X*2) site mixture. Again, the refined La distribution indicates some disorder of the normal La chain that centers the cell face, Fig. 8a. 0–28% occupied La1 site at the normal position, $0,\frac{1}{2},\frac{1}{4}$, centers *X*2 tetrahedra with *d*(La2–*X*2) = 3.24 Å vs. a bond radius sum of 2.90 Å. Additionally, a split 24% occupied position for La3 centered around the pair of *X*2 sites gives each La3 two neighbors at 2.96 Å. The displacement parameters for La1 and La3 are now much more nearly normal. The fact that all La atoms have occupancies of ~25% allows a considerable reduction in what we have conjectured to be destabilizing La–La contacts along *c* axis, 2.74 Å (*c*/2) for the normal

Table 14
Interatomic distances (4.5 Å) in $La_{4.762(5)}Ga_{1.5(1)}Zn_{1.5}$

La1–La3 × 2	0.916(6)	La3–La3	0.91(1)
La1–La3 × 2	1.824(6)	La3–La1	0.916(6)
La1–La1 × 2	2.740(1)	La3–La1	1.824(6)
La1–La1 × 4	3.225(2)	La3–La3	1.83(1)
La1–La3 × 2	3.656(6)	La3–La3 × 2	2.740(1)
La1–La2 × 8	3.9612(8)	La3–*X*2 × 2	2.955(2)
La2–*X*2 × 2	3.2557(9)	La3–La3	3.65(1)
La2–*X*2	3.301(2)	La3–La1	3.656(6)
La2–Ga1 × 2	3.348(7)	La3–*X*2 × 2	3.708(4)
La2–La2	3.435(1)	La3–La2 × 4	3.744(1)
La2–*X*2	3.509(1)	La3–*X*2 × 2	4.328(5)
La2–La2 × 2	3.534(1)	La3–La2 × 4	4.363(3)
La2–La2 × 2	3.671(1)	*X*2–La3 × 2	2.955(2)
La2–La3 × 2	3.744(1)	*X*2–La1 × 2	3.238(2)
La2–La1 × 2	3.9612(8)	*X*2–La2 × 4	3.2557(9)
La2–La2 × 2	4.320(1)	*X*2–La2 × 2	3.301(2)
La2–La3 × 2	4.363(3)	*X*2–La2 × 2	3.509(1)
Ga1–Ga1 × 2	2.740(1)	*X*2–La3 × 2	3.708(4)
Ga1–La1 × 8	3.3481(7)	*X*2–*X*2 × 2	4.209(3)
		*X*2–La3 × 2	4.328(5)

[a] *X* = mixed Ga2, Zn2. La1 and La3 have fractional occupancies of ~28% and 24%, respectively.

positioning vs. 3.38 Å for metallic diameters. Again, the fractional occupancy and apparent disorder in this (sub)cell can be readily accounted for in terms of a rather similar superstructure (or a disorder from intergrowth), as shown in a different style in Fig. 8b for the 2*c* cell. The La–La distances are again very similar and reasonable, 3.70 and 3.69 Å.

Stoichiometric variabilities were not investigated in the two La–Ga–*Z* systems, but these are likely to occur. The upper limit of La content on the side faces would be interesting if the disorder/incommensurate characteristics could be clarified. These La–Sn–*Z* (~W_5Si_3 type) phases have the shortest *c* axes of any of the six compounds considered here, and also the largest electron-per-atom counts, 3.0–2.8 (Table 1). The characters of the two La results seem distinct from the others studied, perhaps influenced by the higher electron count. However, no theoretical efforts to understand W_5Si_3-type structures under the influence of sizable variations in electron count seem to have been published.

4. Conclusions

We have in this paper demonstrated evidence of substantial Ba1 substoichiometry and disorder in the W_5Si_3-type structure of $Ba_{4.81}Pb_3$ and of the existence of only ternary phases in the Ca–Sn–Mg, Ca–Sn–Zn, Ca–Sn–Cu, La–Ga–Al and La–Ga–Zn systems crystallizing in structures closely related to that of W_5Si_3. It is important to note that the quality of all of the refinements is quite respectable in terms of residuals (Table 2). Interestingly, the Mg compound $Ca_4Sn_{3.223(4)}Mg_{0.777}$ has neither the disorder nor short *M*–*M* bonds along the tetrahedral chain and is the most well-behaved among the three Ca–Sn–*Z* structures. The existence of short (~3.0 Å) bonds between atoms in the equivalent of the W1 sites of W_5Si_3 (in tetrahedral chains) is again seen in $Ca_{4.78(2)}Sn_3Zn_{0.70(2)}$, but the Ca sites are now only 66% occupied, and two disordered fragment structures seem plausible. Distortion stabilizes the structure in a lower symmetry space group (*P*4/*mbm*). In $Ca_4Sn_3Cu_{1.30(2)}$, two fractional sites of the smaller copper replaces all the Ca1 atoms and avoids close contacts along the chain, but the interpretation is less intelligible. The La–Ga–Al,Zn phases are both stabilized in the W_5Si_3 structure in a somewhat different manner, (a) by ~25% La in four disordered sequences with reasonable La–La distances together with (b) appreciable substitution of the larger Al or Zn for the Ga atoms that define the enclosing tetrahedra. Incommensurate structures seem probable. These two systems also have notably higher electron concentrations.

References

[1] H. Nowotny, in: P.A. Beck (Ed.), Electronic Structure and Alloy Chemistry of the Transition Metals, InterScience Publishers, New York, 1963, p. 179.
[2] B. Aronnson, Acta. Chem. Scand. 9 (1953) 1107.
[3] P. Villars, L.D. Calvert, Pearson's Handbook of Crystallographic Data, Second ed, ASM International Metals Park, Ohio, 1991, p. 5272.
[4] E. Garcia, J.D. Corbett, Inorg. Chem. 29 (1990) 3274.
[5] Y.U. Kwon, J.D. Corbett, Chem. Mater. 4 (1992) 190.
[6] A.M. Guloy, J.D. Corbett, Inorg. Chem. 32 (1993) 3532.
[7] J.D. Corbett, E. Garcia, A.M. Guloy, W.-M. Hurng, Y.-U. Kwon, E.A. Leon-Escamilla, Chem. Mater. 10 (1998) 2824.
[8] E.A. Leon-Escamilla, J.D. Corbett, Inorg. Chem. 40 (2001) 1226.
[9] E.A. Leon-Escamilla, J.D. Corbett, J. Solid State Chem. 159 (2001) 149.
[10] E.A. Leon-Escamilla, J.D. Corbett, J. Alloys Compd. 265 (1998) 104.
[11] E. Parthé, H. Nowotny, H. Schmid, Monatsch Chem. 86 (1955) 385.
[12] Y.U. Kwon, S.C. Sevov, J.D. Corbett, Chem. Mater. 2 (1990) 550.
[13] H. Kleinke, C. Ruckert, C. Felser, Eur. J. Inorg. Chem. (2000) 315.
[14] J.W. Kaiser, W. Jeitschiko, Z. Anorg. Allg. Chem. 628 (2002) 337.
[15] A.V. Tkachuk, A. Mar, J. Solid State Chem. 177 (2004) 4136.
[16] L. Pauling, Nature of the Chemical Bond, Third ed, Cornell University Press, Ithaca, NY, 1960, p. 403.
[17] A. Palenzona, P. Manfrinetti, M.L. Fornasini, J. Alloys Compd. 280 (1998) 211.
[18] A. Palenzona, P. Manfrinetti, M.L. Fornasini, J. Alloys Compd. 312 (2000) 165.
[19] A.K. Ganguli, A.M. Guloy, E.A. Leon-Escamilla, J.D. Corbett, Inorg. Chem. 32 (1993) 4349.
[20] I.S. Miller, P. Bottcher, J. Alloys Compd. 183 (1992) 98.
[21] J.T. Zhao, J.D. Corbett, J. Alloys Compd. 210 (1994) 1.
[22] Y.-U. Kwon, M.A. Rzeznik, A. Guloy, J.D. Corbett, Chem. Mater. 2 (1990) 546.
[23] J.T. Zhao, J.D. Corbett, Unpublished research.

[24] A.K. Ganguli, A.M. Guloy, J.D. Corbett, J. Solid State Chem. 152 (2000) 474.
[25] B.A. Hunter, LHPM—Rietica Rietveld, version 1.71, Australia, 1997.
[26] N. Walker, B. Stuart, Acta Crystallogr. 39A (1983) l58.
[27] G.M. Sheldrick, SHELXS-86, Universitat Gottingen, Germany, 1986.
[28] TEXSAN, Version 6.0 package, Molecular Structure Corp., The Woodlands, TX, 1990.
[29] SMART, Bruker AXS, Inc., Madison, WI, 1996.
[30] R.H. Blessing, Acta Crystallogr. A 51 (1995) 33.
[31] SHELXTL, Bruker AXS, Inc., Madison, WI, 2000.
[32] J.T. Zhao, J.D. Corbett, Inorg. Chem. 34 (1995) 378.
[33] A.M. Guloy, Ph.D. Thesis, Iowa State University, 1991.
[34] A. Leon-Escamilla, Ph.D. Dissertation, Iowa State University, 1996.
[35] S. Delfino, A. Succone, G. Borzona, R. Ferro, Z. Anorg. Allg. Chem. 503 (1983) 184.
[36] B. Eisenmann, H. Schafer, Z. Naturforsch. 22B (1967) 102.
[37] M. Schlüter, A. Kunst, R. Pöttgen, Z. Anorg. Allg. Chem. 628 (2002) 264l.
[38] P.A. Maggard, J.D. Corbett, Inorg. Chem. 37 (1998) 814.